IEEE Access
Multidisciplinary | Rapid Review | Open Access Journal

IEEE MAGNETICS SOCIETY SECTION

Received 18 May 2022, accepted 11 July 2022, date of publication 19 July 2022, date of current version 25 July 2022.

Digital Object Identifier 10.1109/ACCESS.2022.3192404

RESEARCH ARTICLE

Multi-Fidelity Model-Based Size Optimization of Electric Machines

SUNGHO AHN AND SEUNGJAE MIN, (Member, IEEE)
Department of Automotive Engineering (Automotive-Computer Convergence), Hanyang University, Seoul 04763, South Korea
Corresponding author: Seungjae Min (seungjae@hanyang.ac.kr)

ABSTRACT The multi-modal problem and high computational cost represent challenges in the optimization of electric machines owing to their highly nonlinear electromagnetic response. To overcome these challenges, this paper proposes a multi-fidelity model-based sequential optimization method in which both low- and high-fidelity models are employed in two phases. In phase 1, the reluctance network (RN) is adopted as the low-fidelity model and mainly contributes to alleviating the abovementioned challenges. To overcome the low accuracy of the RN, the optimal design is obtained using a finite element model (FEM) in phase 2. The multi-start strategy and gradient-based algorithm are utilized instead of a heuristic algorithm in all phases to avoid excessive calculations. This mutli-fidelity model concept has an originality compared to previous research that has focused on algorithm development. The effectiveness of the proposed method is validated with two examples, consisting of the TEAM workshop problem 25 and the torque ripple minimization of an interior permanent magnet synchronous motor. The optimal designs and computational time resulting from the proposed method are compared with those of the conventional method, where only a FEM is used during optimization. The results show that the proposed method is remarkable in finding superior optimal designs, while ignoring unimportant local optima. Additionally, it can save up to 90% of the computational time required by the conventional method.

INDEX TERMS Computational efficiency, electric machine, finite element model, multi-fidelity model, multi-modal problem, reluctance network.

I. INTRODUCTION

The geometric parameters of electric machines have been optimized to improve their performances, in terms of electromagnetic force and torque, efficiency and weight. Such optimization requires a nonlinear analysis because of the magnetic saturation effect on the machines. This nonlinear analysis requires a large amount of computational resources as it includes iterative processes. Additionally, nonlinearity causes a multi-modal problem where multiple local optima occur and prohibits obtaining a superior local optimum.

The use of a proper surrogate model reduces the high computational cost by reducing the nonlinear electromagnetic finite element (FE) analysis, which is expensive in optimization [1]. Surrogate models, such as Kriging [2]–[5], the response surface model (RSM) [6], and the radial basis function (RBF) [7]–[9], are selected to approximate the unknown model and are supported by the sampling method. The surrogate model helps accelerate the optimization, as the FE analyses are only conducted at the sampling points. However, the accuracy of the surrogate model depends on the number and distribution of the sample points where the FE analyses are conducted. Though adopting more sample points increases the accuracy, it also requires more time to evaluate the FE model. Heuristic algorithms, such as genetic algorithm (GA) [2], [6]–[11], the pareto archived evolution strategy (PAES) [3], particle swarm optimization (PSO) [4]–[13], the evolutionary strategy algorithm (ESA) [5], and differential evolution (DE) [12] have been used to avoid local optima caused by the multi-modal problem. Because these algorithms are based on stochastic methods, they can perform global optimization to obtain the best or multiple solutions. Some size optimizations examples that use surrogate model and heuristic algorithm to address the computationally

The associate editor coordinating the review of this manuscript and approving it for publication was Philip Pong.

TABLE 1. Categorization of size optimizations of electric machines.

Electric machine	Model	Algorithm	Objective function	Reference
Permanent magnet assisted synchronous reluctance motor	Kriging	GA	Torque ripple	[2]
Switched reluctance motor		PAES	Back-EMF	[3]
Switched reluctance motor		PSO	Torque ripple	[4]
Magnetic actuator		ESA	Average torque	[5]
Linear motor	RSM	GA	Torque ripple	[6]
Interior permanent magnet synchronous motor	RBF	MIGA	Average torque	[7]
Magnetic actuator		NSGA-II	Magnet length	[8]
Magnetic actuator		GA	Force	[9]
Universal motor	FE model	GA	Weight	[10]
Linear generator		GA	Torque ripple	[11]
Interior permanent magnet synchronous motor		DE	Terminal velocity	[12]
Interior permanent magnet synchronous motor		DbIPSO	Total energy	[13]

TABLE 2. Advanced algorithms developed by previous research to handle the multi-modal problem.

Electric machine	Algorithm	Number of variables	Reference
SMES device	m-AINet	3	[14]
SMES device	SANGA	3	[15]
AFPMSM	Climb method	2–3	[16, 17]
IPMSM	Multi-modal Big Bang-Big Crunch	3	[18]
PMa-SynRM	Adaptive-Sampling Kriging Algorithm	2	[19]

expensive and multi-modal problems are categorized in Table 1.

Advanced heuristic algorithms have been developed to handle the multi-modal problem in electromagnetic optimization as listed in Table 2. Campelo *et al*. [14] presented a modified version of an artificial immune network algorithm (m-AINet) that searches for local optima in superconducting magnetic energy storage (SMES) device optimization. Dilettoso and Salerno [15] suggested a self-adaptive niching genetic algorithm (SANGA) coupled with a pattern search to find local optima. These algorithms are applied to electromagnetic problems and allow designers to determine the best solution from local optima. Woo *et al*. [16] introduced a new climb method, employing the Kriging and an evolutionary strategy to propose a novel algorithm that provides a specific number of arbitrary local optima. This algorithm was applied to minimize the cogging torque of an axial flux permanent magnet machine (AFPMSM), and three local solutions were obtained [16], [17]. Moreover, Yoo *et al*. [18] and Son *et al*. [19] suggested and developed a computationally efficient algorithm that was applied for the multi-modal optimization of an interior permanent magnet synchronous motor (IPMSM) and a permanent magnet assisted synchronous reluctance motor (PMa-SynRM). Previous studies have focused on heuristic algorithms to address the multi-modal problem by finding multiple optima. However, a considerable number of FE analyses are still required in heuristic algorithms because of these stochastic properties. Therefore, a surrogate model must be used to reduce the computational time. The quality of the local optima obtained via heuristic algorithm depends on both the hyperparameters of the algorithm and how well the surrogate model represents the response. Accordingly, depending on the optimization problem or response, the design engineer has to select an approximation method to construct an accurate surrogate model as well as the heuristic algorithm hyperparameters.

In this study, the concept of multi-fidelity model-based optimization is proposed to address both the computationally expensive and multi-modal problems while overcoming the surrogate model dependency of previous studies. The multi-fidelity model consists of both a reluctance network (RN) and an FE model, which have different fidelity levels. The proposed optimization method is divided into two sequential phases, where the RN and FE model are used in the first and second phases, respectively. During the entire optimization process of the proposed method, sequential quadratic programming (SQP), which uses a gradient-based algorithm, is adopted for both phases. The proposed multi-fidelity optimization is applied to two numerical examples: a magnetic die press model, known as TEAM workshop problem 25, and an IPMSM, which is used as the traction motor of electric vehicles. In each example, the optimization starts with a sufficient number of initial designs to show that the multi-modal problem is properly addressed. To verify that the proposed method is robust in addressing the multi-modal problem and is computationally efficient, the results are compared with a conventional optimization case that only uses the FE model and SQP.

The remainder of this paper is organized as follows. Section 2 presents the multi-fidelity concept including RN used as a low-fidelity model for electromagnetic analysis and explains how the use of a RN mitigates the multi-modal problem. Additionally, a comparison between the proposed

TABLE 3. similarity between an electric circuit and a reluctance network.

Electric circuit	Reluctance network
Voltage V [V]	Magnetomotive force mmf [A]
Current I [A]	Magnetic flux ϕ [Wb]
Resistance R [Ω]	Reluctance R_m [A/Wb]
$V = IR$	$mmf = \phi R_m$

sequential optimization process and the conventional method is also presented. Section 3 describes the two numerical examples and corresponding results to verify the performance of the proposed optimization method. Finally, section 4 summarizes the study and evaluates the proposed method.

II. MULTI-FIDELITY MODEL AND SEQUENTIAL OPTIMIZATION

A. MULTI-FIDELITY CONCEPT INCLUDING RELUCTANCE NETWORK

The multi-fidelity model is a hybrid concept that properly uses two analysis model with different fidelity level. The multi-fidelity concept can maximize the advantages of each model while mitigating the disadvantages that each model has. FE model is a representative high-fidelity model used for nonlinear electromagnetic analysis because of its high accuracy. However, the FE model requires considerable computational cost especially in an optimization problem. This study includes RN in the multi-fidelity model to improve the computational efficiency and to relieve multi-modal problem.

An RN is a magnetic-circuit-based model that uses similarity to an electric circuit, as presented in Table 3, and is used for magnetic field in various electric machines such as a magnetic gear [20], axial permanent magnet bearingless flywheel machine [21], and permanent magnet eddy current brake [22]. A unit network contains four reluctances and a magnetomotive force induced by a current or permanent magnet; an RN structure is shown in Fig. 1. As the reluctance, shown in Fig. 1(a), is the path through which magnetic flux flows, the flux direction is fixed biaxially in the unit network. The magnetomotive force is caused by the remanent flux density of the permanent magnet or the current in the coil, as shown in Figs. 1(b) and 1(c). A certain domain for electromagnetic analysis can be transformed into a RN, as shown in Fig. 1(d), and its components can be expressed as follows:

$$R_m = \frac{l}{\mu A_m} \tag{1}$$

$$mmf_c = NI \tag{2}$$

$$mmf_{PM} = B_r \frac{l_{PM}}{\mu_{PM}} \tag{3}$$

where the reluctance R_m depends on the cross-sectional area A_m, length l, and permeability μ. The magnetomotive force mmf_c from the current relies on amplitude I and turns N. The permanent magnet also induces force, which is proportional

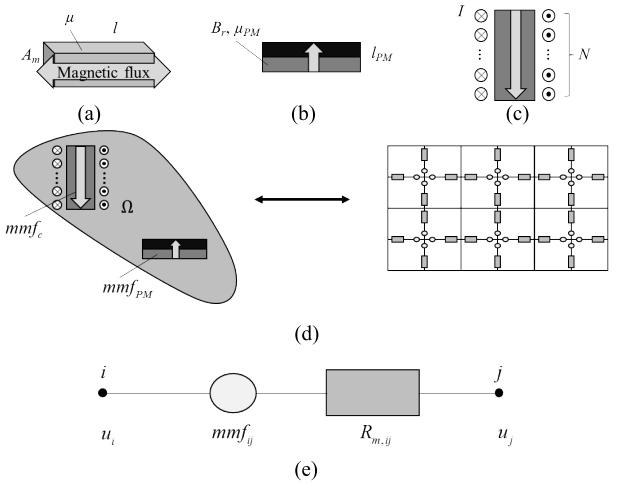

FIGURE 1. Structure of a reluctance network: (a) reluctance, (b) permanent magnet, (c) coils, (d) reluctance network equivalent to the analysis domain and (e) node connections.

to the length in the polar direction l_{PM}, remanent flux density B_r, and inverse of permeability μ_{PM}.

To conduct the electromagnetic analysis using the RN and determine the potential u, Kirchhoff's current law is applied to all nodes i as as follows:

$$\sum_j \frac{1}{R_{m,\,ij}}(u_i - (u_j + mmf_{ij})) = 0 \tag{4}$$

where the subscripts j and ij indicate the nodes adjacent to node i and the forces between nodes i and j, respectively, as shown in Fig. 1(e). Depending on the source of magnetomotive force, mmf_{ij} can be substituted with mmf_c or mmf_{PM}. Then, all equations according to the nodes in the RN are assembled to create the following system equation:

$$PU = F \tag{5}$$

where potential vector U is solved with system matrix P and force vector F. The magnetic flux density B_{ij} through a reluctance that is placed between nodes i and j is calculated as follows:

$$B_{ij} = \frac{u_i - u_j}{R_{m,\,ij}A} \tag{6}$$

The process of assembling and solving the system matrix should be repeated to consider the nonlinearity of the core material by updating the permeability at each iteration [23]. The iterative process continues until the maximum permeability change rate in the core region is negligible.

As the potential value of u_i at each node i in the RN is a scalar, the degree of freedom (DOF) of the RN is quite low, even when compared with an FE model consisting of the same number of nodes. Because a low DOF reduces the time required for assembling and solving the system equations, the main advantage of using an RN for electromagnetic analysis is its computational efficiency. Despite its high computational efficiency, the low DOF produces low-accuracy analysis,

which is a major disadvantage of the RN compared to the FE model. However, the proposed optimization avoids the disadvantage by not using the RN to obtain the final design.

B. MULTI-MODAL RESPONSE RELIEF

The capability to relieve the multi-modal problem is another advantage of employing an RN because the governing equation is different from that of the FE method. To solve the magnetostatic field analysis in the FE method, the Poisson equation containing second derivative term is derived from Maxwell's equations, and is given by

$$\nabla \times \left(\frac{1}{\mu} (\nabla \times A) \right) = J \tag{7}$$

where J is the current density vector. Then, the magnetic vector potential A is determined using weak form in the analysis domain. Unlike the FE method, Ohm's law in Table 3 was used as the governing equation in the RN and did not include the derivative term. This relatively linear aspect of the governing equation contributes to alleviating the multi-modal problem.

In electromagnetic analysis, the flux density is an important physical value because the main properties of an electric machine, such as force, torque, and energy, are calculated using the flux density. Using the FE model, the flux density B at each node is calculated as follows:

$$B = \nabla \times A \tag{8}$$

and B at any set of coordinates is represented by a shape function. This characteristic of the FE model enables it to precisely reflect the magnetic nonlinearity that occurs in electric machines. However, when using an RN, the direction of the flux density in a unit network is fixed *a priori* during the modeling process. The orthogonally fixed direction of the flux density in the RN restricts its ability to represent the nonlinearity of electric machines. Therefore, the magnetic properties resulting from the RN appear more linear, compared to those of the FE model, and using the RN alleviates the multi-modal problem.

Relief of the multi-modal problem by the RN is investigated via the TEAM workshop problem 25 [24], which is the magnetic die press model optimization, as represented in Fig. 2. The optimization contains four design variables: inner die radius (R1), major and minor ellipse radius (L2 and L3, respectively), and outer die length (L4). Multi-fidelity models were constructed as illustrated in Fig. 3, and the DOFs of the RN and FE model were 193 and 27,310, respectively. Using each model, the objective function was defined as follows:

$$f = \sum_{i=1}^{10} \left\{ \left(B_{xip} - B_{xio}\right)^2 + \left(B_{yip} - B_{yio}\right)^2 \right\} \tag{9}$$

f is calculated and investigated to determine how different the multi-modal response is according to the model used. B_{xip} and B_{yip} are the flux densities in the x- and y-direction, respectively, and are evaluated at 10 points, where the e-f curve is equally divided. B_{xio} and B_{yio} are the target flux densities in the x- and y-directions, respectively, at the same points, and the total current induced to the coil is 4253 ampere-turns.

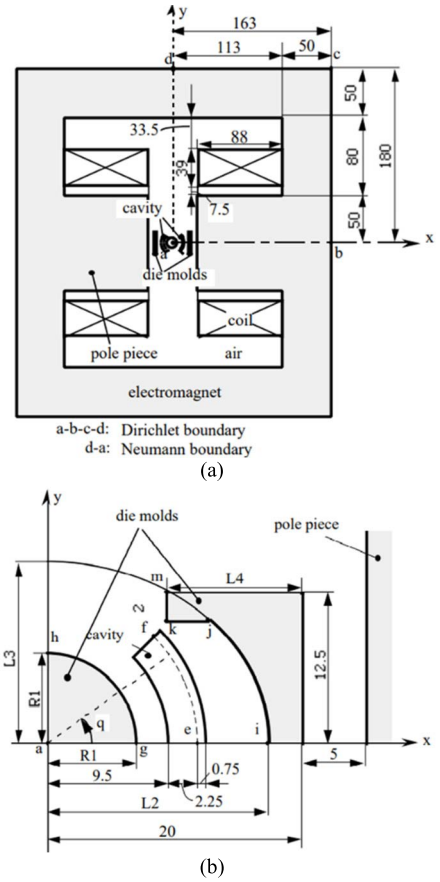

FIGURE 2. Quarter symmetric die press model [24]: (a) entire view and (b) enlarged view.

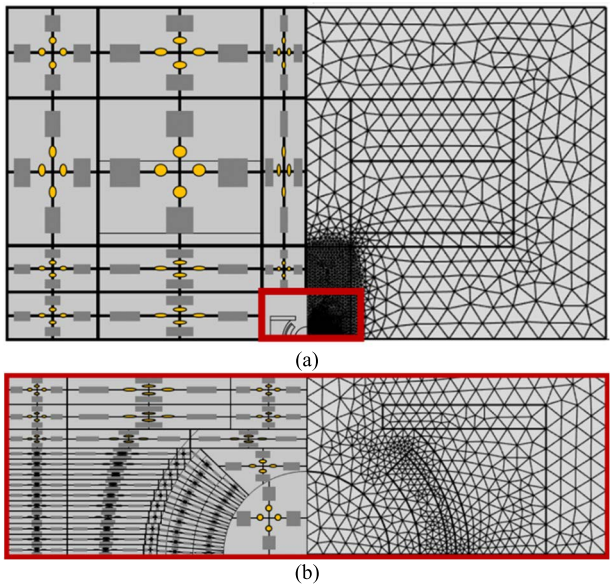

FIGURE 3. Multi-fidelity die press models: (a) entire view and (b) enlarged view of the region outlined by the red box in (a).

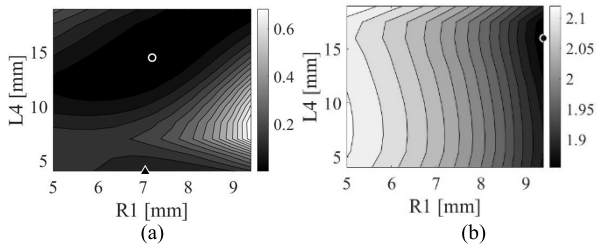

FIGURE 4. Contours of the objective function evaluated by the (a) FE model and (b) RN.

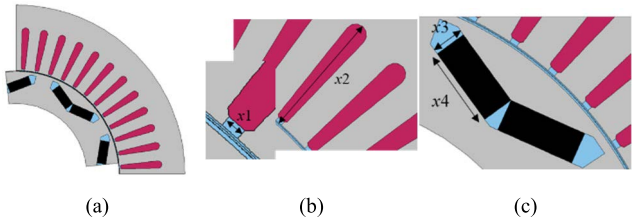

FIGURE 5. IPMSM configurations: (a) quarter periodic model, (b) stator and (c) rotor.

The multi-modal response of the objective function and relief by the RN are shown in Fig. 4. The objective function was evaluated at 121 gridded points using each model to illustrate the contours, where two insensitive variables of the ellipse were fixed [25]. The gridded points were determined by splitting each R1 and L4 boundary evenly into 11 levels, and L2 and L3 were fixed at 18.0 and 14.0 mm, respectively. Fixed values are selected to display the contours where the multi-modal response relief is dominant. The minimum point is marked by a circle in each panel of Fig. 4. Additionally, it is shown that the FE model produces another local minimum (marked by a triangle in Fig. 4(a)), while the RN does not. This graphical representation also demonstrates the fidelity difference between the two models, showing that the objective function dependence on R1 is not well reflected in RN. Therefore, the trade-off relationship between accuracy and multi-modal response relief is successfully visualized.

The effectiveness of RN in relieving the multi-modal response was also investigated in an IPMSM, which is a rotating electric machine used for traction in the PRIUS 2004 electric vehicle. The motor has 48 slots with distributed three-phase winding, and 8 poles, and its cross section is shown in Fig. 5 [26]. The design variables consist of slot opening width($x1$), slot height($x2$), magnet thickness($x3$), and magnet width($x4$), which are compared in Fig. 6 for the RN and FE model. The DOFs of the RN and FE model are 2,449 and 19,370, respectively. The torque ripple contours are constructed using different fidelity models at the rated operating point [27], where currents in the d- and q-axis are -184 and 151.6 A, respectively.

The multi-modal response mitigated by the RN is shown in Fig. 7, where $x2$ and $x4$ are fixed at 40.2 and 18.8 mm, respectively. The data used for the figure were evaluated at

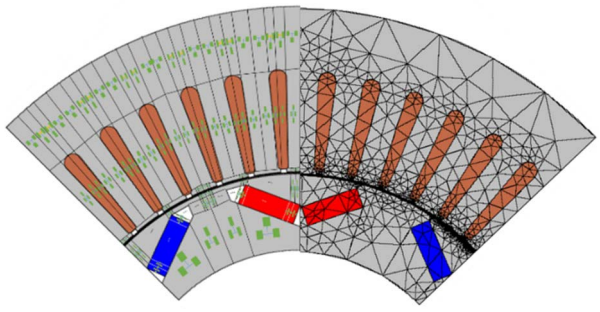

FIGURE 6. Comparison of the multi-fidelity IPMSM model between the RN (left) and FE model (right).

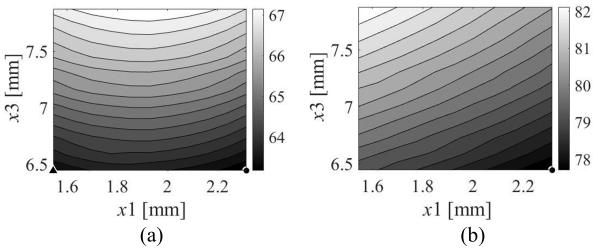

FIGURE 7. Torque ripple evaluated by the (a) FE model and (b) RN.

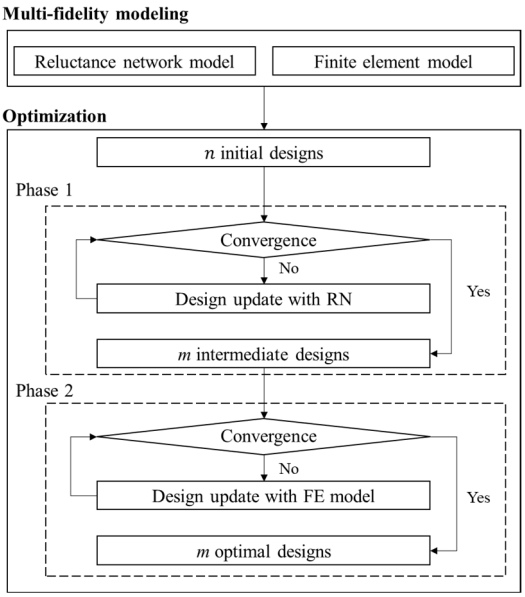

FIGURE 8. Optimization procedure of the proposed method.

121 gridded points, which were selected in the same manner as in the previous machine. In both panels of Fig. 7, the minimum point is located in the lower right corner. However, the FE model produces another local minimum located in the lower left corner in Fig. 7(a). Additionally, comparing the surfaces produced by each model, the nonlinearity of the torque ripple according to $x1$ appears to be more dominant in the FE model than in the RN. Accordingly, it is shown that a relatively linear response in the RN relieves the multi-modal problem in the optimization.

C. SEQUENTIAL OPTIMIZATION

The proposed multi-fidelity model-based optimization method proceeds following the sequence, shown in Fig. 8. In phase 1, n initial designs are updated with the RN and optimized to m optimal designs, defined as intermediate designs in this study. The main purpose of using the RN is to alleviate the multi-modal problem by shifting the initial designs toward a reduced number of intermediate designs. Furthermore, the time spent conducting n trials in phase 1 is insignificant compared to phase 2, owing to the low DOF of the RN. Starting with the reduced m intermediate designs, the optimal designs are obtained by updating the high-fidelity FE model in the phase 2. Finally, n and m optimizations are conducted in each phase using the RN and FE model, respectively. The proposed method adopts a gradient-based algorithm in both phases, rather than a stochastic or population-based heuristic algorithm, to avoid unnecessary evaluations of the FE model. In this study, SQP was selected, which has the advantages of generality, robustness, and efficiency [28].

Although recent studies have optimized electric machines such as linear machines [29] and permanent magnet motors [30]–[33] using only an RN alone, the results were verified via FE analysis. This means that a high-fidelity model is required even if the optimizations are conducted using only a low-fidelity RN. Moreover, it is not guaranteed that the design obtained from the RN is a local optimum, even if the design has a better objective function than the initial design. In this study, because the final design is obtained with a high-fidelity FE model, the low-accuracy problem that arises from the RN is avoided.

To confirm the effectiveness of the proposed method in alleviating the multi-modal problem and in terms of computational efficiency, its results were compared with those obtained from the conventional method, which only uses a high-fidelity FE model and skips phase 1. The conventional method does not adopt a surrogate model because a fair comparison would not be possible due to the response error between the surrogate and FE models caused by the approximation method.

III. NUMERICAL EXAMPLES

A. TEAM WORKSHOP PROBLEM 25

To verify the proposed method performance, a size optimization of a magnetic die press model, known as the TEAM workshop problem 25, was conducted. The optimization problem is defined as follows:

$$\begin{aligned} \underset{x}{\text{minimize}} \quad & f = \sum_{i=1}^{10} \left\{ \left(B_{xip} - B_{xio}\right)^2 + \left(B_{yip} - B_{yio}\right)^2 \right\} \\ \text{subject to} \quad & x_{lb} \le x \le x_{ub} \end{aligned} \tag{10}$$

where x_{lb} and x_{ub} are the lower and upper bounds of the design variable vector x, respectively, as listed in Table 4.

To confirm that the multi-modal problem is mitigated by the proposed method, the optimization starts with 81 initial designs, which are selected by fully combining of all variables with 3 levels. Using the conventional method, 81 optimizations supported by the FE model were required to find the best local minimum. However, using the proposed method, 81 initial designs were reduced to 3 intermediate designs that resulted from phase 1, as shown in Fig. 9. Then, only three optimizations were conducted in phase 2, and optimal designs were obtained using the FE model. As a result of the proposed optimization method, three optimal designs were obtained and compared to those of the conventional method, as shown in Fig. 10. The conventional method produced five optimal designs, including the results of the proposed method, and the details of both optimizations are listed in Table 5. The values in the last column of Table 5 are based on the number of initial designs. As opposed to the results of the conventional method, the proposed method avoided local optimum #4 and #5, which are unnecessary designs because of the high objective function. Additionally, 14 out of the 15 initial designs that converged to optimum #3 in the conventional method were shifted to a better optimum (#1 or #2) in the proposed method. These results indicate that the proposed method helps relieve the multi-modal problem.

The computational time required to find all local optima using conventional and proposed methods is shown in Fig. 11 (computer configuration: Intel Core i7-3770K, 3.5 GHz, 12 GB memory). In the conventional cases, 331 min were

TABLE 4. Bounds of design variables in magnetic actuator example.

Design variable [mm]	x_{lb}	x_{ub}
R1	5.0	9.4
L2	12.6	18.0
L3	14.0	45.0
L4	4.0	19.0

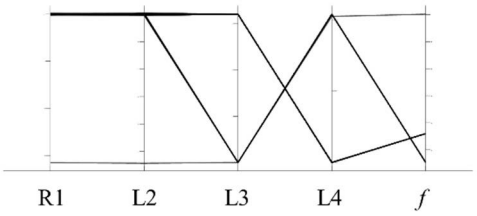

FIGURE 9. Intermediate designs obtained from phase 1 in the proposed method.

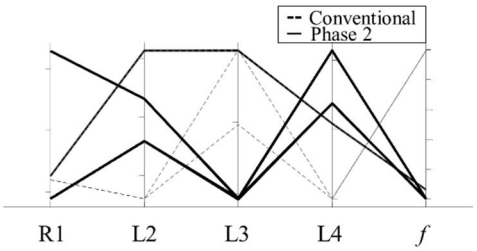

FIGURE 10. Optimal designs comparison between the conventional and proposed methods.

TABLE 5. optimization results from the conventional and proposed methods for the magnetic actuator example.

Optimum	$f(\times 10^{-4})$	R1 [mm]	L2 [mm]	L3 [mm]	L4 [mm]	Conventional / proposed
#1	3.67	9.3	14.3	14.0	19.0	24 / 16
#2	4.01	6.9	13.6	14.0	13.7	40 / 64
#3	64.2	7.3	15.1	45.0	11.6	15 / 1
#4	995	7.2	12.6	45.0	4.0	1 / 0
#5	995	7.2	12.6	29.5	4.0	1 / 0

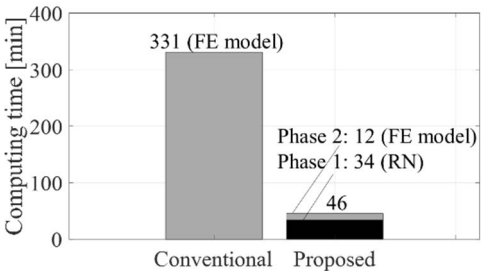

FIGURE 11. Computational time required for the TEAM workshop problem 25 optimization by the conventional and proposed methods.

TABLE 6. Bounds of design variables in the IPMSM example.

Design variable [mm]	x_{lb}	Initial	x_{ub}
$x1$	1.5	1.9	2.3
$x2$	26.8	33.5	40.2
$x3$	6.4	7.2	7.9
$x4$	16.1	17.9	18.8

consumed for 81 optimizations with the FE model. By contrast, the proposed method required 34 and 12 min for phase 1 and 2, respectively. From the computational time comparison, it is confirmed that the proposed method has high computational efficiency.

B. INTERIOR PERMANENT MAGNET SYNCHRONOUS MOTOR

The proposed method was also applied to the torque ripple minimization of an IPMSM as high torque ripple causes vibration and noise during motor operation [34], [35]. The bounds of the design variables are set to 40% of the initial design to maintain the shape change limitation, as listed in Table 6. These variables affect the shape of the tooth and poles, which are mainly related to the torque characteristics. In this optimization, two inequality constraints were included to preserve the average torque T_{avg} and to prevent the magnet area A_{PM} from increasing. The average torque preservation helps to maintain the acceleration performance of motor. It is preferred to use less amount of magnet because large magnet increases the material cost. The formulation is defined as follows:

$$\begin{aligned} \underset{x}{\text{minimize}} \quad & f = T_{ripple} \\ \text{subject to} \quad & g_1 = T_0 - T_{avg} \le 0 \end{aligned}$$

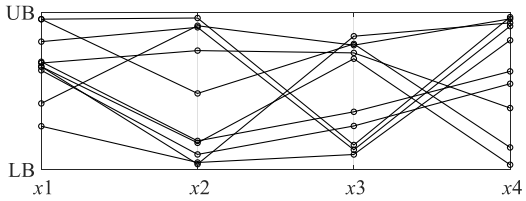

FIGURE 12. Randomly selected 10 initial designs.

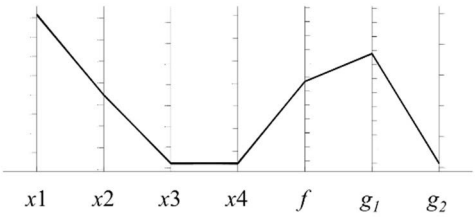

FIGURE 13. Intermediate designs obtained from phase 1 in the proposed method.

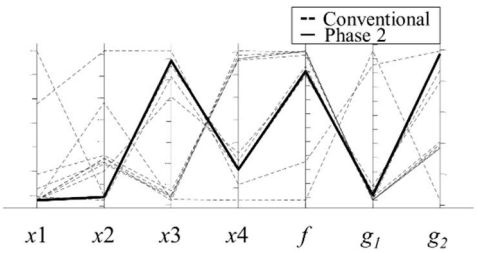

FIGURE 14. Optimal designs comparison between the conventional and proposed methods.

$$\begin{aligned} & g_2 = A_{PM} - A_{0,PM} \le 0 \\ & x_{lb} \le x \le x_{ub} \end{aligned} \tag{11}$$

where the T_{avg} and A_{PM} are determined by the initial design and are set to 358 Nm and 128 mm^2, respectively.

In the constrained optimization, the offset difference between the RN and FE model responses can affect the intermediate design obtained in phase 1 of the proposed method. For example, the average torque calculated by the RN based on the initial design is 308 Nm, which is 14% lower than that of the FE model. If T_0 is fixed at 358 Nm in the phase 1, the feasible region may shrink depending on the offset difference. To make g_1 effective in the proposed optimization, T_0 was set to 308 Nm in phase 1 and 358 Nm in phase 2.

TABLE 7. Optimization results from the conventional and proposed methods for the IPMSM example.

Optimum	f	g_1	$g_2(\times 10^{-6})$	$x1$ [mm]	$x2$ [mm]	$x3$ [mm]	$x4$ [mm]	Conventional / proposed
#1	63.0	0.68	-0.7	1.5	30.7	7.8	16.4	3 / 10
#2	53.8	21.1	-24.2	1.5	32.9	6.5	16.1	1 / 0
#3	56.6	19.1	-0.19	1.6	34.1	7.9	16.2	1 / 0
#4	64.4	0.06	-15.8	1.5	31.6	6.5	17.4	5 / 0

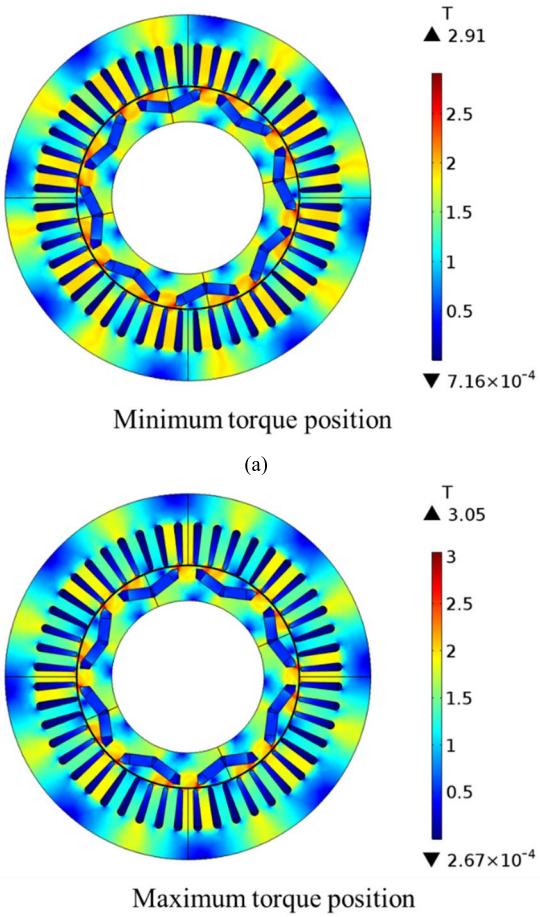

FIGURE 15. Magnetic flux distribution of the optimal motor #1 at different rotor positions: (a) 45° and (b) 90° in electrical angle.

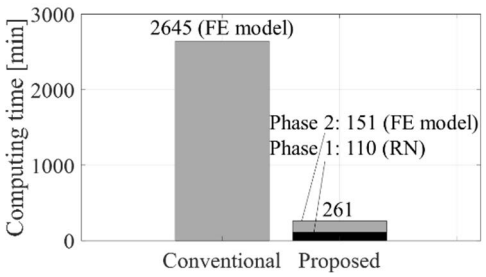

FIGURE 16. Computational time required for the IPMSM optimization by the conventional and proposed methods.

As opposed to the previous example, 10 initial designs were randomly selected within the bounds of the design variables to assume a situation in which the multi-modal problem was practically alleviated. All initial designs are displayed in Fig. 12, where some of them may not satisfy the constraints. Starting from all initial designs, phase 1 makes all designs converge to a single optimum, as shown in Fig. 13. After proceeding to the phase 2, the optimal design is compared to the conventional cases containing four local optima, as shown in Fig. 14. Additionally, the data of optimal designs, such as the objective function and constraint violations, are summarized in Table 7, where optima #1 and #4 are feasible designs considering that the violations of the first constraint are sufficiently low to be neglected. Optimum #1 is the best design because the objective function is lower and the second constraint is more active than in optimum #4. The magnetic flux distribution of the optimum #1 is evaluated by FE model at the minimum and maximum torque positions, as shown in Fig. 15. In the maximum torque position, the flux density at the rotor rib exceeds 3.0 T that is extreme value at the motor, however, such result comes from the linear extrapolation of limited BH-curve data of core not from any simulation error. Therefore, as the best optimal design was obtained using the proposed method, regardless of the starting points, it is confirmed that the proposed method is effective in alleviating the multi-modal problem.

When performing ten optimizations using the conventional method, it took 2,645 min to obtain four different designs consisting of the best optimum, one feasible, and two infeasible solutions, as shown in Fig. 16. Conversely, the proposed method required only 261 min, which is less than one-hundredth of that required by the conventional method. In this example, the convergence of the ten initial designs into one in phase 1 contributes to the high computational efficiency of the proposed method.

IV. CONCLUSION

In this paper, a multi-fidelity model-based size optimization method is proposed to alleviate the multi-modal problem in electromagnetics and to make the process more computationally efficient. This multi-fidelity model concept is a novel approach to handle the problems in electromagnetic machine optimization because previous research only has developed algorithms. The performance of the proposed method was verified using two numerical examples,

the TEAM workshop problem 25 and IPMSM optimization. The manner in which the RN relieved the multi-modal problem was investigated in terms of different governing equations from the FE model. To utilize the advantages of different fidelity models and reduce their disadvantages, the proposed optimization method adopted a two-phase sequential procedure. Using the RN in the phase 1 relieved the multi-modal problem and increased its computational efficiency. Moreover, the low accuracy of the RN was overcome by obtaining the optimal design from the FE model in phase 2.

In both examples, phase 1 successfully reduced all initial designs to a few intermediate designs. In the first example, 81 initial designs were reduced to three intermediate designs. Additionally, 10 randomly selected initial designs in the second example converged to a single design through phase 1. Comparing the optimal designs obtained after proceeding with phase 2 to those obtained using the conventional method, it is shown that the multi-modal problem was relieved. Furthermore, the proposed method does not miss the best local optimum for each optimization problem. To verify the computational efficiency of the proposed method, the total computational time required for the optimization was compared. The proposed method saved 86% and 90% of the computational time required for each example compared with the conventional method. The high computational efficiency of the proposed method arises from the role of phase 1, which reduces the number of expensive optimizations required in phase 2.

Although the proposed optimization alleviates the multi-modal problem and is computationally efficient in all examples, its performance may depend on the fidelity of the RN. The finer the discretization of the RN, the smaller the computational efficiency advantage. Thus, proper RN discretization is important to maintain the advantages of the proposed method.

REFERENCES

[1] G. Lei, J. Zhu, Y. Guo, C. Liu, and B. Ma, "A review of design optimization methods for electrical machines," *Energies*, vol. 10, no. 12, p. 1962, Nov. 2017.

[2] H.-C. Liu, I.-G. Kim, Y. J. Oh, J. Lee, and S.-C. Go, "Design of permanent magnet-assisted synchronous reluctance motor for maximized back-EMF and torque ripple reduction," *IEEE Trans. Magn.*, vol. 53, no. 6, pp. 1–4, Jun. 2017.

[3] S. I. Nabeta, I. E. Chabu, L. Lebensztajn, D. A. P. Correa, W. M. D. Silva, and K. Hameyer, "Mitigation of the torque ripple of a switched reluctance motor through a multiobjective optimization," *IEEE Trans. Magn.*, vol. 44, no. 6, pp. 1018–1021, May 2008.

[4] Z. Ren, D. Zhang, and C.-S. Koh, "Multi-objective worst-case scenario robust optimal design of switched reluctance motor incorporated with FEM and Kriging," in *Proc. Int. Conf. Electr. Mach. Syst. (ICEMS)*, Mar. 2013, pp. 716–719.

[5] S.-K. Hong, J.-S. Ro, and H.-K. Jung, "Optimal design of a novel permanent magnetic actuator using evolutionary strategy algorithm and Kriging meta-model," *J. Electr. Eng. Technol.*, vol. 9, no. 2, pp. 471–477, Mar. 2014.

[6] D. Zarko, S. Stipetic, M. Martinovic, M. Kovacic, T. Jercic, and Z. Hanic, "Reduction of computational efforts in finite element-based permanent magnet traction motor optimization," *IEEE Trans. Ind. Electron.*, vol. 65, no. 2, pp. 1799–1807, Feb. 2018.

[7] J. Hao, S. Suo, Y. Yang, Y. Wang, W. Wang, and X. Chen, "Optimization of torque ripples in an interior permanent magnet synchronous motor based on the orthogonal experimental method and MIGA and RBF neural networks," *IEEE Access*, vol. 8, pp. 27202–27209, 2020.

[8] J. Jiang, H. Lin, and S. Fang, "Multi-objective optimization of a permanent magnet actuator for high voltage vacuum circuit breaker based on adaptive surrogate modeling technique," *Energies*, vol. 12, no. 24, p. 4695, Dec. 2019.

[9] Y.-K. Son, Y.-M. You, and B.-I. Kwon, "Optimal design to increase thrust force in electro-magnetic linear actuator for fatigue and durability test machine," *IEEE Trans. Magn.*, vol. 47, no. 10, pp. 4294–4297, Oct. 2011.

[10] G. Papa, B. Korousic-Seljak, B. Benedicic, and T. Kmecl, "Universal motor efficiency improvement using evolutionary optimization," *IEEE Trans. Ind. Electron.*, vol. 50, no. 3, pp. 602–611, Jun. 2003.

[11] O. Farrok, M. R. Islam, Y. Guo, J. Zhu, and W. Xu, "A novel design procedure for designing linear generators," *IEEE Trans. Ind. Electron.*, vol. 65, no. 2, pp. 1846–1854, Feb. 2018.

[12] H. M. Hasanien, A. S. Abd-Rabou, and S. M. Sakr, "Design optimization of transverse flux linear motor for weight reduction and performance improvement using response surface methodology and genetic algorithms," *IEEE Trans. Energy Convers.*, vol. 25, no. 3, pp. 598–605, Sep. 2010.

[13] J. H. Lee, J.-W. Kim, J.-Y. Song, D.-W. Kim, Y.-J. Kim, and S.-Y. Jung, "Distance-based intelligent particle swarm optimization for optimal design of permanent magnet synchronous machine," *IEEE Trans. Magn.*, vol. 53, no. 6, pp. 1–4, Jun. 2017.

[14] F. Campelo, F. G. Guimaraes, H. Igarashi, J. A. Ramirez, and S. Noguchi, "A modified immune network algorithm for multimodal electromagnetic problems," *IEEE Trans. Magn.*, vol. 42, no. 4, pp. 1111–1114, Mar. 2006.

[15] E. Dilettoso and N. Salerno, "A self-adaptive niching genetic algorithm for multimodal optimization of electromagnetic devices," *IEEE Trans. Magn.*, vol. 42, no. 4, pp. 1203–1206, Mar. 2006.

[16] D.-K. Woo, J.-H. Choi, M. Ali, and H.-K. Jung, "A novel multimodal optimization algorithm applied to electromagnetic optimization," *IEEE Trans. Magn.*, vol. 47, no. 6, pp. 1667–1673, Jan. 2011.

[17] D.-K. Lim, D.-K. Woo, I.-W. Kim, J.-S. Ro, and H.-K. Jung, "Cogging torque minimization of a dual-type axial-flux permanent magnet motor using a novel optimization algorithm," *IEEE Trans. Magn.*, vol. 49, no. 9, pp. 5106–5111, Apr. 2013.

[18] C.-H. Yoo, D.-K. Lim, and H.-K. Jung, "A novel multimodal optimization algorithm for the design of electromagnetic machines," *IEEE Trans. Magn.*, vol. 52, no. 3, pp. 1–4, Sep. 2015.

[19] J.-C. Son, J.-M. Ahn, J. Lim, and D.-K. Lim, "Optimal design of PMa-SynRM for electric vehicles exploiting adaptive-sampling Kriging algorithm," *IEEE Access*, vol. 9, pp. 41174–41183, 2021.

[20] Y.-C. Wu and B.-S. Jian, "Magnetic field analysis of a coaxial magnetic gear mechanism by two-dimensional equivalent magnetic circuit network method and finite-element method," *Appl. Math. Model.*, vol. 39, no. 19, pp. 5746–5758, Oct. 2015.

[21] Z. Zhu, H. Zhu, X. Li, J. Zhu, and M. Cheng, "Dynamic equivalent magnetic network analysis of an axial PM bearingless flywheel machine," *IEEE Access*, vol. 9, pp. 32425–32435, 2021.

[22] M. Gulec, P. Lindh, M. Aydin, and J. Pyrhonen, "Cost minimization of a permanent magnet eddy current brake by multiobjective particle swarm optimization based on nonlinear reluctance network modeling," *IEEE Access*, vol. 9, pp. 157361–157370, 2021.

[23] D. J. Gómez, A. L. Rodríguez, I. Villar, A. López-de-Heredia, I. Etxeberria-Otadui, and Z. Q. Zhu, "Experimental validation of an enhanced permeance network model for embedded magnet synchronous machines," *Electr. Power Syst. Res.*, vol. 140, pp. 836–845, Nov. 2016.

[24] N. Takahashi. *Optimization of Die Press Model: TEAM Workshop Problem 25*. Accessed: Dec. 2021. [Online]. Available: http://www.compumag.org/jsite/images/stories/TEAM/problem25.pdf

[25] L. Lebensztajn, C. A. R. Marretto, M. C. Costa, and J.-L. Coulomb, "Kriging: A useful tool for electromagnetic device optimization," *IEEE Trans. Magn.*, vol. 40, no. 2, pp. 1196–1199, Apr. 2004.

[26] R. H. Staunton, S. C. Nelson, P. J. Otaduy, J. M. McKeever, J. M. Bailey, S. Das, and R. L. Smith, "PM motor parametric design analyses for a hybrid electric vehicle traction drive application," Oak Ridge Nat. Lab., Oak Ridge, TN, USA, Tech. Rep. ORNL/TM-2004/217, 2004.
[27] Z. Yang, F. Shang, I. P. Brown, and M. Krishnamurthy, "Comparative study of interior permanent magnet, induction, and switched reluctance motor drives for EV and HEV applications," *IEEE Trans. Transport. Electrific.*, vol. 1, no. 3, pp. 245–254, Aug. 2015.
[28] J. S. Arora, *Introduction to Optimum Design*, 2nd ed. San Diego, CA, USA: Elsevier, 2004.
[29] E. M. Barhoumi, F. Wurtz, C. Chillet, B. B. Salah, and O. Chadebec, "Efficient reluctance network formulation for modeling design and optimization of linear hybrid motor," *IEEE Trans. Magn.*, vol. 52, no. 3, pp. 1–4, Mar. 2016.
[30] G. Xu, G. Liu, S. Jiang, and Q. Chen, "Analysis of a hybrid rotor permanent magnet motor based on equivalent magnetic network," *IEEE Trans. Magn.*, vol. 54, no. 4, pp. 1–9, Apr. 2018.
[31] C. Lopez-Torres, A. Garcia, J.-R. Riba, G. Lux, and L. Romeral, "Computationally efficient design and optimization approach of PMa-SynRM in frequent operating Torque–Speed range," *IEEE Trans. Energy Convers.*, vol. 33, no. 4, pp. 1776–1786, Apr. 2018.
[32] C. L. Torres, T. Michalski, A. G. Espinosa, and L. Romeral, "Fast optimization of the magnetic model by means of reluctance network for PMa-SynRM," in *Proc. 42nd Annu. Conf. IEEE Ind. Electron. Soc. (IECON)*, Oct. 2016, pp. 1642–1647.
[33] D. Cao, W. Zhao, J. Ji, and Y. Wang, "Parametric equivalent magnetic network modeling approach for multiobjective optimization of PM machine," *IEEE Trans. Ind. Electron.*, vol. 68, no. 8, pp. 6619–6629, Jul. 2020.
[34] Y. Kong, M. Lin, M. Yin, and L. Hao, "Rotor structure on reducing demagnetization of magnet and torque ripple in a PMa-synRM with ferrite permanent magnet," *IEEE Trans. Magn.*, vol. 54, no. 11, pp. 1–5, Nov. 2018.
[35] V. Simon-Sempere, A. Simon-Gomez, M. Burgos-Payan, and J.-R. Cerquides-Bueno, "Optimisation of magnet shape for cogging torque reduction in axial-flux permanent-magnet motors," *IEEE Trans. Energy Convers.*, vol. 36, no. 4, pp. 2825–2838, Dec. 2021.

SUNGHO AHN was born in Incheon, South Korea. He received the B.S. and M.S. degrees in automotive engineering from Hanyang University, Seoul, South Korea, in 2020 and 2022, respectively.

His research interests include coupled electromagnetic-thermal analysis of interior permanent magnet synchronous motor, computationally efficient design of electric machine using equivalent circuit models, and multi-physics optimization of electrified propulsion systems.

SEUNGJAE MIN (Member, IEEE) received the B.S. and M.S. degrees in mechanical engineering from Seoul National University, Seoul, South Korea, in 1989 and 1991, respectively, and the Ph.D. degree in mechanical engineering from the University of Michigan, Ann Arbor, in 1997.

From 1997 to 1999, he was a Research Associate at the Naval Architecture and Ocean Engineering Department, University of Tokyo. From 1999 to 2010, he was an Assistant and an Associate Professor at the Mechanical Engineering Department. Since 2010, he has been a Professor with the Automotive Engineering Department, Hanyang University, Seoul. His research interests include physics-based and/or data-driven modeling, simulation and optimization, structural design, and CAE.

Dr. Min was a recipient of the CAE and Applied Mechanics Awards for Excellence of the Korean Society of Mechanical Engineers, in 2020. He is an Executive Committee Member of Asian Society of Structural and Multidisciplinary Optimization (ASSMO).